Molecular Physics, 2013
Vol. 111, Nos. 12–13, 1855–1864, http://dx.doi.org/10.1080/00268976.2013.810791

Taylor & Francis
Taylor & Francis Group

INVITED ARTICLE

Manipulating the motion of polar molecules with microwave radiation

Simon Merz[a,b,c], Claudia Brieger[c,†], Nicolas Vanhaecke[c,d], Gerard Meijer[c,e] and Melanie Schnell[a,b,*]

[a]*Center for Free–Electron Laser Science, Notkestrasse 85, 22607 Hamburg, Germany;* [b]*Max–Planck–Institut für Kernphysik, Saupfercheckweg 1, 69117 Heidelberg, Germany;* [c]*Fritz–Haber–Institut der Max–Planck–Gesellschaft, Faradayweg 4–6, 14195 Berlin, Germany;* [d]*Laboratoire Aimé Cotton, CNRS, Bâtiment 505, Université Paris–Sud, 91405 Orsay, France;* [e]*Radboud University Nijmegen, Institute for Molecules and Materials, Heyendaalseweg 135, 6525 AJ Nijmegen, the Netherlands*

(*Received 28 January 2013; final version received 28 May 2013*)

Microwave radiation coupled into a cylindrically symmetric resonator is used to focus, guide, decelerate, and accelerate ammonia molecules in high-field-seeking states. In a first series of measurements, we demonstrate that the focal length of a microwave lens is directly proportional to the molecules' velocity and to the inverse of the fourth root of the microwave power. In a second series of measurements employing a modified set-up, we use a multi-stage decelerator exploiting the $TE_{1,1,12}$ mode of a cylindrical resonator and various switching schemes. We can deliberately choose between spatial focusing and velocity focusing while guiding, and we demonstrate kinetic energy reduction by as much as 30% of a 12 m/s slow packet of molecules utilising the 12 deceleration stages.

Keywords: cold molecules; microwave deceleration; ac Stark effect

1. Introduction

Our abilities to manipulate and control beams of neutral polar molecules in the gas phase using external fields have been greatly improved over the past decade [1–4]. Nowadays, one can generate packets of state-selected molecules with well-controlled spatial and velocity distributions. These experiments mark an important milestone in recent molecular physics and physical chemistry research. Well-defined packets of cold molecules enable further refinement of spectroscopy experiments by increasing the interaction time of the probing field, thus nicely demonstrating its remarkable power for increasing the resolution of a spectroscopic experiment [5,6]. Furthermore, controlled beams have been used to investigate (in)elastic scattering of molecules with low velocities and thus low collision energies and high resolution [7,8]. For small polar molecules, such as ammonia or the OH radical, these advances rely on the development and constant improvement of Stark decelerators [9]. Here, the interaction between polar molecules and inhomogeneous electric fields is employed, i.e., the dc Stark effect. Molecules that decrease their Stark energy with decreasing electric field strength and thus are attracted by a minimum of the electric field (so-called low-field seekers) experience stable and efficient deceleration in a Stark decelerator. This works, however, for molecules in low-field-seeking states only and thus limits the species that can be manipulated and thoroughly investigated to rather small molecules and prevents manipulation of the molecular ground states as well as that of larger, more complex molecules that are high-field seekers.

The first experiments that specifically manipulated the motion of molecules in high-field-seeking states used the dynamic-focusing method, invented to manipulate the motion of charged particles in synchrotrons in the early 1950s. Based on dynamic focusing, that is often also called alternating-gradient focusing, guides [10–13], decelerators [14,15], and traps [16,17] for polar molecules in high-field-seeking states have recently been developed. Even though alternating-gradient focusing and deceleration have been demonstrated by several groups in the recent past, it remains experimentally very demanding, and most experiments of this type have been discontinued. By using an electrostatic deflector similar to the electric analogue of a Stern–Gerlach deflector, however, large molecules can be quantum state– and conformer–selected, an important prerequisite for novel alignment and orientation experiments [18].

Another approach for the manipulation of molecules in high-field-seeking states is the use of strong optical fields to manipulate the motion of polarisable molecules in, for instance, counter-propagating laser beams [19]. With optical fields one can produce three-dimensional field maxima in free space, which is impossible with dc fields due to

*Corresponding author. Email: melanie.schnell@asg.mpg.de
†Present address: Freie Universität Berlin, Institut für Chemie und Biochemie, Takustrasse 3, 14195 Berlin, Germany.

Earnshaw's theorem [20]. This way, non-polar neutral molecules can also be addressed. The large field gradients available in laser beams enable rapid deceleration or acceleration, but only a small fraction of molecules from a typical pulsed molecule source can be captured at a time due to the very small interaction volume spanned by the laser beams.

We recently presented a promising alternative route to obtain slow molecules in high-field-seeking states relying on their manipulation with microwave fields. Due to their long wavelengths, microwave fields offer a significantly larger interaction volume of several mm^3, comparable to the emittance of a pulsed valve or a buffer-gas cooled beam as well as the spatial acceptance of common Stark decelerators and molecule traps. Microwave fields in a cavity offer the great advantage that they can be tailored to exhibit a variety of well-defined electric-field distributions. For specific resonance modes of the cavities, in particular the ground mode, three-dimensional field maxima can be generated in free space. At the same time, a high-quality cavity provides the necessary field strength to manipulate the motion of neutral polar molecules.

In the microwave manipulation experiments presented here, we make use of the permanent electric dipole moment of a molecule by exploiting its interaction with a strong microwave field that is close to a transition frequency in the molecule. This interaction is described by the ac Stark effect. Thus far, a deflector for CsF molecules [21] has been realised, and we have demonstrated a microwave lens [22], microwave guiding, and deceleration/acceleration of slow ammonia molecules in a microwave resonator [23]. In this paper, we further characterise this promising technique and present new focusing, guiding, and deceleration results of ammonia molecules in high-field-seeking states. We also discuss the limitations of our current set-up and present ideas of how to overcome these.

2. The AC Stark effect

The interaction of polar molecules with the microwave field relies on the ac Stark effect. It has particular properties that differ from the well-known dc Stark effect. We describe a rotational state of ammonia by $|J, K, M\rangle$, where J is the total angular momentum quantum number, K is the quantum number associated with the projection of the angular momentum onto the C_3 symmetry axis of ammonia and M is the quantum number considering the projection of the angular momentum onto a specific axis within the laboratory system, i.e., it specifies the orientation of the molecule in space. Within such a rotational state of the vibronic ground state of $^{14}NH_3$, we consider a two-level system consisting of the two levels of the inversion doublet. In the frame of the rotating wave approximation, the ac Stark shift is given by the eigenenergies of the 2×2 Hamiltonian matrix and reads

$$W_{ac\text{-}Stark} = \pm\sqrt{\left(\frac{h\Delta}{2}\right)^2 + \left(\mu E_{MW}\frac{KM}{2J(J+1)}\right)^2} \mp \frac{h\Delta}{2}. \quad (1)$$

Here, μ is the permanent dipole moment, E_{MW} is the electric field strength of the microwave field and Δ is the detuning $\Delta = \nu_{MW} - \nu_0$ of the microwave frequency ν_{MW} with respect to the molecular transition frequency ν_0. The electric field strength of the microwave field in the cylindrically symmetric resonator we use is given by

$$E_{MW} = \sqrt{\frac{4.2}{\pi\epsilon_0}\frac{QP_{MW}}{\nu_{1,1,l}V}}, \quad (2)$$

where $\nu_{1,1,l}$ is the resonance frequency of the $TE_{1,1,l}$ mode used for focusing, guiding, deceleration, and acceleration, which is also the ground mode of that particular type of resonator. l is the mode number in longitudinal direction, V is the resonator volume, Q the quality factor, P_{MW} is the microwave power coupled into the resonator, and ϵ_0 the dielectric constant. The factor 4.2 arises from field normalisation in the cylindrically symmetric cavity. In the experiments discussed in this article, we are exploiting the inversion transition in the rovibrational ground state of $^{14}NH_3$ at $\nu_0 = 23.695$ GHz. A small detuning of 50–100 MHz leads to linear ac Stark shifts at already low field strengths, in particular, when compared to the Stark shift of ammonia in dc fields.

As long as the changes in electric field strength experienced by the molecules are sufficiently slow, the molecules remain adiabatically in the eigenstate of the Hamiltonian that they were initially populating. Quantitatively, this is fulfilled as long as the relative changes of the Rabi frequency Ω (defined by $\frac{\mu E_{MW}}{\hbar}\frac{KM}{2J(J+1)}$) occurs on much slower time scales than the Rabi oscillation, which is always the case in our experiment due to the low velocities of the molecules and the slow switching times. As an example, the worst case scenario would be effects due to switching the microwave fields. The ringdown time of the resonator and the operating speed of the switch give an overall decay time of about 10 μs, which is much slower than the period of a Rabi oscillation (of the order of 4 ns at 1.4 kV/cm).

Note that the sign of the detuning determines the sign of the square root in Equation (1). By choosing the sign of the detuning, the sign of the ac Stark shift and thus the behaviour of the molecules in the field are determined. We use a well-defined molecular packet generated by Stark deceleration as input to our microwave resonator (*vide infra*). These molecules exclusively populate the upper level of the inversion transition of the vibronic ground state of para-ammonia that is low-field seeking in dc fields. For a positive detuning ($\Delta > 0$), however, these molecules are high-field seeking in the ac microwave field, while molecules in the

corresponding lower level of the inversion transition are ac low-field seeking. For negative detuning ($\Delta < 0$), the situation would be reversed. We can use this tunability to our advantage, which is also described in the following.

3. The experimental set-up

The complete beam experiment is shown in Figure 1(A) and consists of a cooled pulsed valve, an electrostatic hexapole, a Stark decelerator, the microwave decelerator, and an ion detection zone. The pulsed valve (General Valve Series 9) generates a supersonic beam of cold ammonia molecules ($^{14}NH_3$) seeded in xenon with rotational and translational temperatures of about 2 K. The molecular beam is skimmed, i.e., only molecules with small transverse velocity components are able to pass the skimmer that also serves as a differential pumping stage. An electrostatic hexapole focuses the dc low-field-seeking molecules in the upper inversion-doublet component of the rovibronic ground state of para-ammonia into the Stark decelerator. The Stark decelerator produces slow packets of about 10^5 ammonia molecules with an extension of $2 \times 2 \times 2$ mm^3 and a tunable longitudinal velocity. For a detailed description of Stark deceleration of ammonia molecules see for example [24]. For our microwave manipulation experiments, we use individual packets with mean velocities ranging from 12 to 50 m/s, as discussed below. The longitudinal velocity distribution is about ± 10 m/s.

The slow packet of molecules is coupled into the 120 mm long microwave resonator that is located 8 mm further downstream (Figure 1(A)). Finally, the molecules are resonantly photo-ionised with a focused UV laser beam

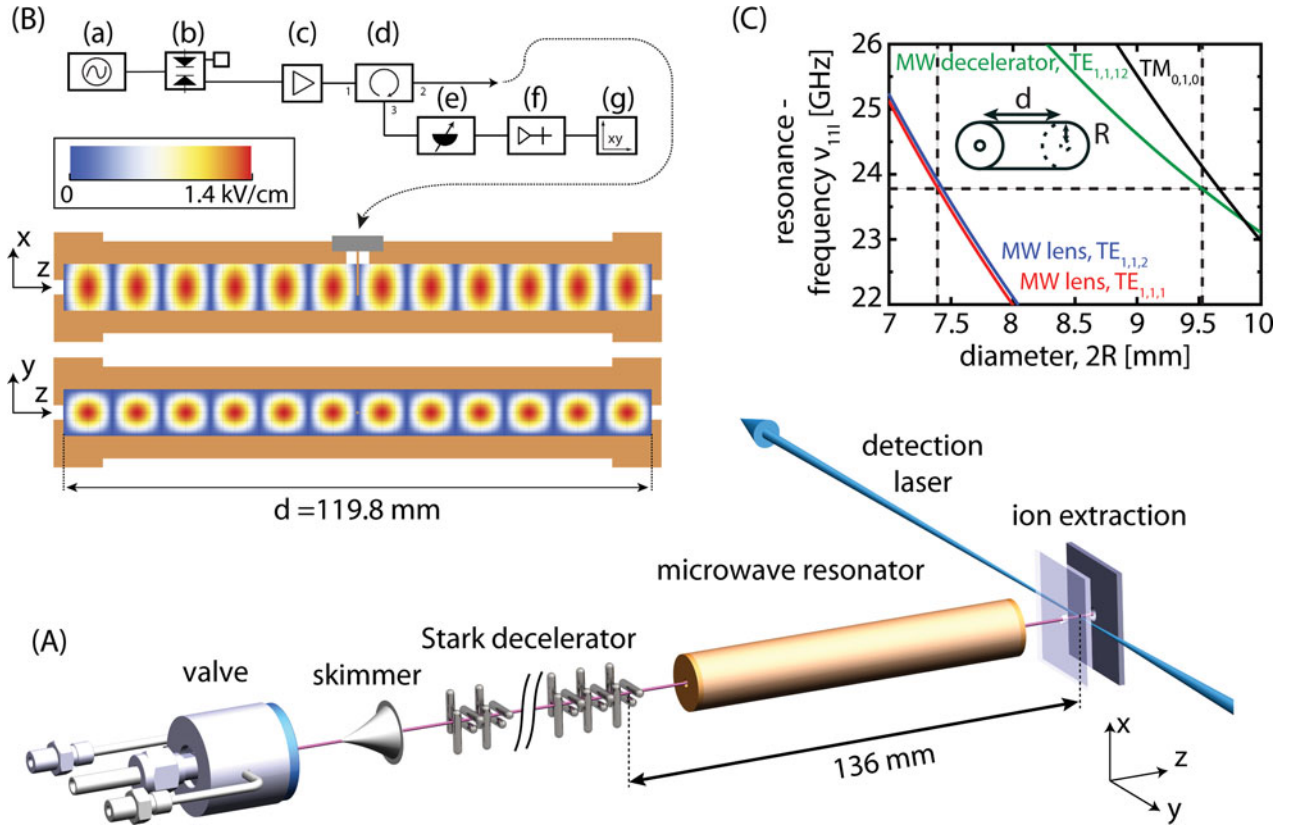

Figure 1. (A): The molecular beam experiment consisting of a pulsed valve, an electrostatic hexapole, the Stark decelerator, the microwave resonator, and the ion detection. (Note that the electrostatic hexapole is not shown in the scheme.) A packet of slow molecules emitted by the Stark decelerator travels through the copper resonator and is detected using resonant photo-ionisation. (B): Schematic overview of the microwave electronics: (a) signal generator SMR27 (1 kHz–27 GHz, Rohde & Schwarz), (b) fast SP–DT pin-diode switch SFB–0526 (Sierra Microwave), (c) power amplifier MKU–2410 A (30 dB gain, maximum output power 40 dBm, Kuhne elektronic), (d) circulator SMC1826 (18–26 GHz, Sierra Microwave), (e) adjustable attenuator AF868-10 (14–26 GHz, Advanced Technical Materials), (f) detector diode 8473C (0.01–26.5 GHz, Agilent), (g) oscilloscope (Tektronix), as well as a scheme of the microwave resonator with contour plots of the electric field of the $TE_{1,1,12}$ mode at $P_{MW} = 3$ W of microwave power. (C) shows the calculated resonance frequencies $\nu_{1,1,l}$ of the cylindrically symmetric microwave resonators depending on the inner diameter $2R$ of the cavities. The resonance frequency of the next higher mode, the $TM_{0,1,0}$ mode, is also shown in each of the three resonators for comparison reasons. The horizontal dashed line indicates the inversion transition frequency of the $|J, K\rangle = |1, 1\rangle$ state in $^{14}NH_3$, and the vertical lines indicate the diameters of the cavities used in the experiments.

(2+1 REMPI). The ionisation zone is located another 8 mm downstream from the microwave decelerator. The parent ions are detected with a compact linear time-of-flight mass spectrometer.

4. The cylindrically symmetric microwave resonators

We used a set of cylindrically symmetric copper resonators that were especially designed for the respective experiments. For guiding and deceleration, for example, the resonator consists of a 119.8 mm long copper cylinder with an inner diameter of 9.57 mm at room temperature. All resonators are closed by two endcaps that are 2 mm thick and exhibit 3 mm diameter holes for the molecules to enter and leave the resonator. They are machined from oxygen-free copper (OFE) to ensure good conductivity. Since the power dissipation of the microwave field is dominated by Ohmic losses in the surface of the resonator walls, i.e., the surrounding conductor, the quality factor Q of the resonator scales with the square root of the conductivity σ ($Q \propto \sqrt{\sigma}$). For oxygen-free copper, σ is about $58 \cdot 10^6$ S/m at room temperature; it increases by a factor of 8 to about $460 \cdot 10^6$ S/m at 77 K (liquid nitrogen temperature) [25].

Please note that in the following the z direction is always directed along the symmetry axis of the resonator that also coincides with the molecular beam axis. The modes in a cylindrically symmetric resonator are solutions to the three-dimensional wave equation and have to fulfil the boundary conditions $\hat{n} \times \vec{E} = 0$ and $\hat{n} \cdot \vec{B} = 0$ at the perfectly conducting surface of the resonator, with $\vec{E}$ and $\vec{B}$ being the electric and magnetic fields, respectively. A complete set of solutions is commonly given by all the different transverse-electric (TE) and transverse-magnetic (TM) modes. The former have no electric field component along the longitudinal direction, while the latter have no longitudinal magnetic field component. Since the transverse fields can be derived from the longitudinal fields,

$$B_z = B_0 J_m \left(x'_{nm} \frac{\rho}{R} \right) \cos(m\phi) \sin\left(\frac{l\pi z}{d} \right) \qquad (3)$$

describes the $\mathrm{TE}_{n,m,l}$ modes in cylindrical coordinates. With

$$E_z = E_0 J_m \left(x_{nm} \frac{\rho}{R} \right) \cos(m\phi) \cos\left(\frac{l\pi z}{d} \right), \qquad (4)$$

the field of the $\mathrm{TM}_{n,m,l}$ modes can be derived. n,m are mode numbers in transverse and l is a mode number in longitudinal direction, respectively. E_0 is the maximum electric field strength, B_0 is the maximum magnetic flux, J_m is the mth order Bessel function of the first kind, d is the length and R the radius of the cylindrically symmetric cavity. x_{nm} and x'_{nm} are the nth roots of the Bessel function J_m and its first derivative, respectively ($J_m(x_{nm}) = 0$ and ($J'_m(x'_{nm}) = 0$)).

The fundamental mode of a cylindrically symmetric resonator with $d \gg R$ is the $\mathrm{TE}_{1,1,l}$ mode (see also Figure 1). It exhibits one field maximum at the centre of the resonator's transverse plane and is thus well-suited for manipulating molecules in ac high-field-seeking states. The $\mathrm{TE}_{1,1,l}$ mode features l consecutive field maxima in the z direction. Note that although the resonator is cylindrically symmetric, this is not the case for the respective field. It has a maximum at the azimuth $\phi = 0$ and a minimum at $\pi/2$ (see also Figure 1). While we use the $l = 1$ and $l = 2$ modes for the rather static process of microwave focusing [22], we use $l = 12$ for microwave guiding and deceleration [23] and switch the fields. The resonators are designed such that the corresponding $\mathrm{TE}_{1,1,l}$ modes are blue-detuned ($\Delta > 0$) by about $\Delta = 50$–70 MHz with respect to the molecular resonance ν_0. In vacuum, the resonance frequency of a $\mathrm{TE}_{1,1,l}$ mode is given by:

$$\nu_{1,1,l} = \frac{c}{2\pi} \sqrt{\frac{x'^2_{11}}{R^2} + \frac{l^2\pi^2}{d^2}}, \qquad (5)$$

where $x'_{11} \approx 1.841$ is the first root of the first derivative of the Bessel function ($J'_1(x'_{11}) = 0$) and c is the speed of light. From this, it becomes obvious that the inner diameter R of the cavity has to be very precisely machined. A change in R of only 10 μm leads to a shift of the resonance frequency of the $\mathrm{TE}_{1,1,12}$ mode by as much as 15 MHz, while the same change in cavity length d results in a shift of less than 1 MHz.

As mentioned above, we use three different cylindrically symmetric microwave resonators, tailored according to the respective experiments, i.e., for applying the $\mathrm{TE}_{1,1,1}$, the $\mathrm{TE}_{1,1,2}$, and the $\mathrm{TE}_{1,1,12}$ modes, respectively. For example, the resonance frequency of the $\mathrm{TE}_{1,1,12}$ mode is detuned by $\Delta = +58$ MHz at liquid-nitrogen temperatures for a 119.8 mm long microwave cavity, with an inner diameter of precisely 9.57 mm. The two cavities used in the focusing experiments have not been cooled. Both cavities are 120.0 mm long. The corresponding detunings are $\Delta = +66$ MHz for the $\mathrm{TE}_{1,1,1}$ mode (inner diameter 7.41 mm) and $\Delta = +71$ MHz for the $\mathrm{TE}_{1,1,2}$ mode (inner diameter 7.43 mm). The microwave radiation is coupled into the resonators via thin copper wires of 3.2 to 6.5 mm length that serve as dipole antennas with varying thicknesses from 0.1 to 0.5 mm. The antenna dimensions depend on the wavelength and the character of the resonator mode to be excited. For $\mathrm{TE}_{1,1,l}$ modes with even l, coupling can be easily achieved in the centre of the cavity, i.e., at a field node. For the resonator exploiting the $\mathrm{TE}_{1,1,1}$ mode, however, the antenna is positioned as close as possible to one of its edges to minimise field disturbances. The quality factors Q of the resonators are of the order of several thousands as determined by the full–width at half–maximum (FWHM) of the cavity resonance. For the

$TE_{1,1,1}$ mode, a Q of about 3500 can be achieved, while for the $TE_{1,1,2}$ mode a Q value of 5200 was measured. Both values were determined at room temperature. The microwave decelerator cavity is cooled to liquid nitrogen temperatures, resulting in a quality factor of $Q \approx 9100$ ($TE_{1,1,12}$ mode).

A schematic overview of the electronic set-up used for microwave focusing and deceleration is given in Figure 1(B). Microwave radiation is generated by a signal generator. A fast single-pull double-throw (SP-DT) pin-diode switch is used to generate well-defined microwave pulses as described in the following section. The amplifier is centred at 23.7 GHz and provides 30 dB gain with a maximum output power of 40 dBm (10 W). A subsequent circulator protects the amplifier from back reflection at the high-frequency vacuum feedthrough or at the cavity when the frequency mismatches the cavity's resonance frequency. It guides the reflected power from the cavity to a detector diode, thus providing also a measure for the frequency match of the generator output with respect to the resonance frequency of the microwave resonator. In the present set-up we capacitively couple about 3 W of microwave power into the microwave field, resulting in a maximum electric field strength of about 1.4 kV/cm in the cylindrically symmetric resonator, according to Equation (2).

5. Experimental results

For focusing, the microwave field is on for the whole time that the molecular packet is inside the resonator, which we here refer to as a time-independent microwave field since we perform no active switching of the field. For guiding, decelerating, and accelerating polar molecules, we need to introduce switched microwave fields. For the sake of simplicity, here we call these microwave fields time-dependent. In all experiments described in the following, we use packets of Stark-decelerated ammonia molecules with controlled longitudinal velocities ranging from 12 m/s to 50 m/s as input to our microwave decelerator. The time origin of the experimental results is defined as the time when the Stark decelerator is switched off. As described in the experimental set-up (Figure 1), the molecules have to travel a total distance of about 136 mm from the end of the Stark decelerator to the detection region.

When the microwave field is on for the whole time that the molecular packet is inside the resonator, i.e., when time-independent fields are used, the molecules are confined in *transverse* directions. The microwave field acts like a positive lens on the ac high-field-seeking $^{14}NH_3$ molecules [22]. Figure 2(A) shows the experimental results for focusing ammonia molecules with different mean velocities of 50 m/s, 35 m/s, and 25 m/s in their $|J, K\rangle = |1, 1\rangle$ state using the $TE_{1,1,1}$ mode, i.e., with only one field maximum on the resonator axis. The ammonia density is measured as a function of the flight time of the molecular packet from the exit of the Stark decelerator to the detection region (about

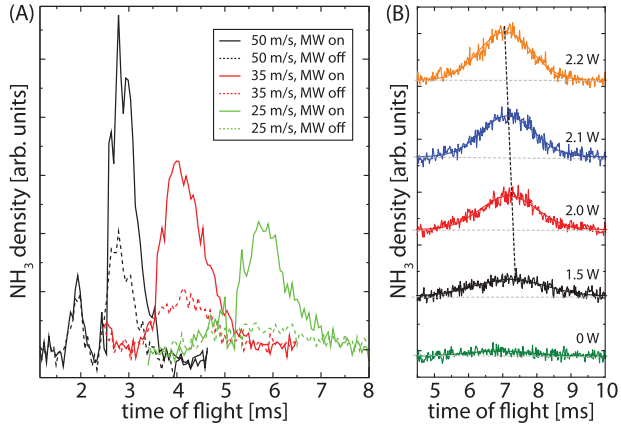

Figure 2. Microwave focusing of decelerated ammonia molecules in the $|J, K\rangle = |1, 1\rangle$ state as a function of their flight time from the Stark decelerator exit to the detection region (136 mm): (A) For three different velocities: 50 m/s (black), 35 m/s (red), and 25 m/s (green). Dashed curves represent measurements with microwave radiation turned off. (B) For 20 m/s slow ammonia molecules but different microwave input power. Bold curves correspond to Gaussian-type fits to the experimental data.

136 mm). For all three measurements, the microwave input power is $P_{MW} = 3$ W. All curves show a significant increase in signal intensity compared to the measurements when the microwave radiation has been turned off (dashed lines). For 50 m/s, this amounts to an increase of about a factor of 2.5 compared to factors of 3 and 6 for 35 m/s and 25 m/s, respectively. The different widths of the packets in the time-of-flight profile originate from the different mean velocities of the packets and from the fact that the microwave field has only a net effect on the transverse motion of the molecules, while their forward motion is almost free flight without any bunching effect on the longitudinal motion. In the measurements for the 50 m/s slow molecules an additional peak at 2 ms is visible. In the Stark decelerator, these molecules experienced one deceleration stage less so that they have a velocity of about 70 m/s. The transverse focusing effect for this considerably higher initial velocity is much weaker, as can be understood from Equations (6) and (7) (*vide infra*).

In Figure 2(B), similar measurements are displayed for ammonia molecules with a mean velocity of about 20 m/s, but with varying microwave powers coupled into the $TE_{1,1,2}$ mode. It is not only the intensity that decreases with decreasing microwave power, but the position of the peak maximum is slightly shifted towards later arrival times and thus slower molecules. This clearly indicates that for different microwave powers different molecule velocities and thus different fractions of the molecular packet will be focused best.

Figure 3(A) shows the dependence of the observed signal on the microwave power P_{MW} for different detection times corresponding to different molecular velocities. Although a velocity distribution has to be considered

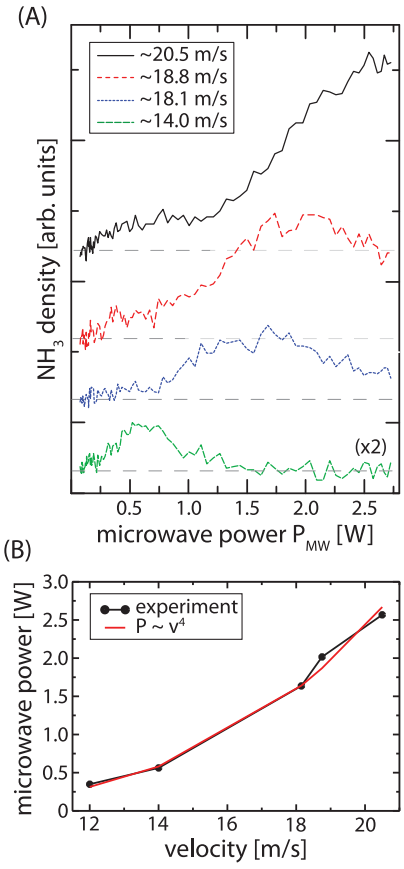

Figure 3. (A) Density of $^{14}NH_3$ molecules as a function of the microwave power P_{MW} for four different observation times and thus molecule velocities. The bottom trace is scaled by a factor of 2 for better visibility. (B) The optimum microwave power in Watt as a function of the corresponding molecule velocity. The black curve (with dots) shows the experimentally obtained data, while the red solid curve gives a fit to the experimental data according to Equation (6).

for each given detection time, we will give the velocity of the molecules in the corresponding synchronous packet here, i.e., the packet that contains the synchronous molecules, since it is the dominant contribution. For all curves, we find a steep increase in signal intensity with increasing microwave power. For molecules travelling with $v_z = 20.5$ m/s, a maximum occurs around 2.6 W, when the overlap of the focus area and the detection area are maximum for the corresponding molecule velocity. (The beam waist of the detection laser amounts to about 100 μm.) By further increasing the microwave power P_{MW} the focus area will be shifted outside the detection area towards the microwave resonator. Over-focusing is observed. This becomes even more apparent for molecules with $v_z \approx 18.8$ m/s for which the maximum is located around 2.0 W. For $v_z \approx 18.1$ m/s and $v_z \approx 14.0$ m/s slow molecules, the maximum is further shifted to 1.6 W and 0.56 W, respectively. Based on Newton's equations of motion and neglecting the anharmonicity in the potential due to the detuning in Equation (1), the focal length L of our microwave lens is proportional to the longitudinal velocity v_z and the microwave power P_{MW} according to

$$L = A(\phi)\frac{v_z}{\sqrt[4]{P_{MW}}}. \tag{6}$$

Here, $A(\phi)$ is a proportionality factor that can be written as

$$A(\phi) = 2\pi^2\sqrt{\frac{J(J+1)}{\mu M K x_{11}'^2}\frac{m_{mol}R^3}{\sin^2\phi + 3\cos^2\phi}}\sqrt[4]{\frac{d\nu_{1,1,l}\epsilon_0}{4.2Q}}, \tag{7}$$

to a good approximation. ϕ is the azimuthal coordinate of a molecule in the microwave resonator. It is not averaged out since ϕ is decoupled from the radial motion and the azimuthal forces are rather weak. J is the total angular momentum quantum number, m_{mol} the mass of the molecules, R the inner radius of the microwave resonator, μ the molecular dipole moment, $x'_{11} \approx 1.841$ the first root of the first derivative of the Bessel function $J'_1(x)$, d the length of the lens, $\nu_{1,1,l}$ the resonance frequency of the corresponding $TE_{1,1,l}$ mode, and Q the quality factor of the resonator. For the $TE_{1,1,2}$ mode of the described resonator (see Section 4), using ammonia $^{14}NH_3$ and the detection laser intersecting the transverse plane at $\phi = 37°$, the set-up is the most sensitive to focusing in the ($\phi = 127°$,z)-plane. From Equation (7) we get $A(127°) \approx 6.5 \times 10^{-3}\ \sqrt[4]{\text{W}}\text{sec}$. This proportionality is nicely followed by our experiments, as seen from Figure 3(B). It displays the microwave power, P_{MW}, needed to optimally focus various longitudinal velocities v_z, and a fit according to Equation (6). Based on our measurements $\frac{v_z}{\sqrt[4]{P}}$ amounts to about 16 $\frac{\text{m}}{\sqrt[4]{\text{W}}\text{sec}}$ that results in a theoretical focal length of $L \approx 104$ mm. Considering the assumption of a harmonic potential, this value is in good agreement with the actual distance of $L \approx 136$ mm.

Motion control in the *longitudinal* direction can be achieved by switching the microwave fields on and off with an appropriate time sequence, i.e., by introducing time dependency. The different switching schemes for guiding, acceleration, and deceleration are displayed in Figure 4 and are explained in more detail in the following. $^{14}NH_3$ molecules in the upper component of the $|J, K\rangle = |1, 1\rangle$ inversion doublet experience a potential in a blue-detuned microwave field ($\Delta > 0$) that resembles the shape of the negative of the electric field, since the ac Stark shift is approximately linear for the microwave field strengths we use. For better describing the switching sequences, we introduce the concept of the synchronous molecule. It is a fictitious molecule travelling along the symmetry axis of the microwave decelerator with the exact initial longitudinal velocity we want to manipulate. The potential that this synchronous molecule experiences is displayed in Figure 4. In the longitudinal direction, it is almost perfectly harmonic.

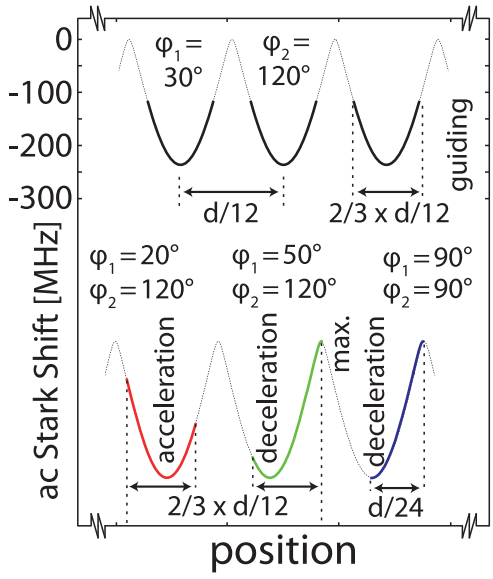

Figure 4. Potential that a $^{14}NH_3$ molecule in the upper component of the $|J, K\rangle = |1, 1\rangle$ inversion doublet ($MK = 1$) experiences when travelling along the symmetry axis of the resonator. The corresponding switching schemes used for guiding, decelerating, and accelerating the molecules are also indicated (bold lines).

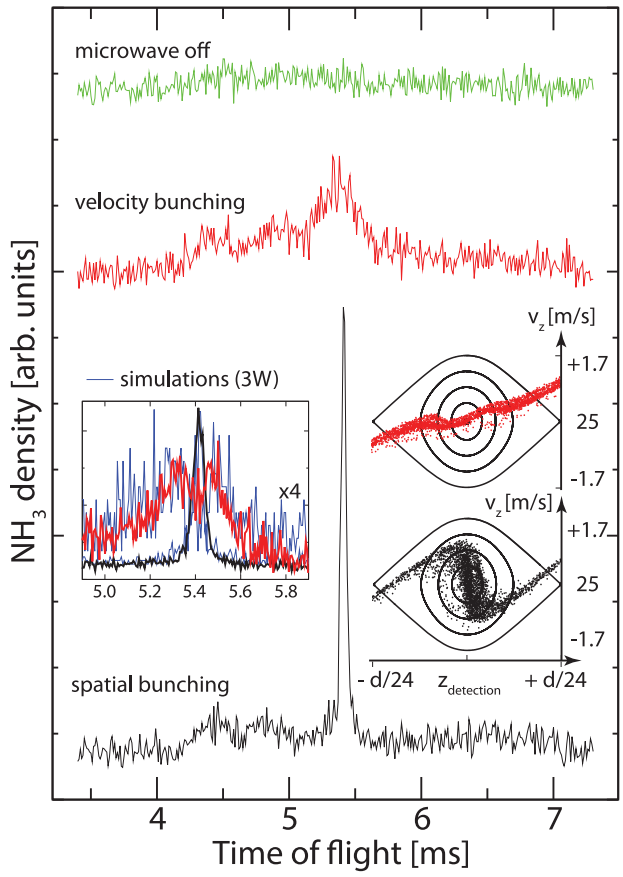

Figure 5. Observed time-of-flight distributions for 25 m/s slow ammonia molecules, detected behind the microwave decelerator. The upper trace shows the ammonia density when the microwave field is off. The middle trace is recorded with a guiding sequence for velocity focusing while the bottom trace shows the time-of-flight distribution for spatial bunching. The different traces have been given an offset for clarity. The inset on the left shows a zoom into the time-of-flight profiles for the spatial bunching and the velocity bunching with higher averaging and smaller time steps (5 μs). The blue traces are the results of simulations for both cases. The velocity-bunching trace and the corresponding simulation trace are scaled by a factor 4 for clarity. The insets on the right show the longitudinal phase-space distribution of the molecular packets in the detection zone for velocity (red, top picture) and spatial bunching (black, bottom picture).

If a constant microwave field is applied, the molecules are converting ac Stark energy to kinetic energy or vice versa so that the net influence on its kinetic energy is zero and only a transverse focusing is achieved. Thus, to decelerate polar molecules, the microwave fields have to be switched on and off such that the overall extraction of kinetic energy overcompensates the gain of kinetic energy. The switching schemes are described using the picture of phase angles. These are defined as follows: in each stage that is a single potential well, the fields are switched on at a position z_1 that corresponds to a phase angle $\phi_1 = 180^\circ \cdot z_1/(d/12)$ (with d being the length of the resonator) and kept on for the time that the synchronous molecule needs to travel to $z_1 + \Delta z$. We can also express the 'microwave duration' Δz in terms of a corresponding angle $\Delta\phi = 180^\circ \cdot \Delta z/(d/12)$. If multiple switching per stage is necessary, we have to introduce an additional index i to denote the switching cycles within a single stage ($\phi_{1,i}$, $\Delta\phi_i$, ...). The maximum duration for the fields that can be turned on per stage is 180° ($\phi_1 = 0^\circ$ and $\Delta\phi = 180^\circ$), which corresponds to the lens mode.

In the first series of measurements, we have explored the guiding mode of operation. The applied fields are switched such that the net effect on the longitudinal velocity of the synchronous molecule is zero. However, molecules that are ahead of the synchronous molecule experience a decelerating force, while slower molecules are accelerated. This way, the molecular packet is kept confined also in longitudinal direction. The results are shown in Figure 5 for an ammonia packet travelling with a mean longitudinal velocity of 25 m/s. For the upper trace, the microwave field is turned off. Barely any ion signal is visible, since the length of the cavity exceeds the diameter of the opening in the exit cap by almost a factor of 40, while the mean longitudinal velocity is just five times larger than the mean transverse velocity. As a result, most of the molecules collide with the copper walls inside the cavity and do not contribute to the ion yield detected behind the resonator. The bottom trace displays the resulting ammonia distribution, when using the $\phi_1 = 30^\circ$ and $\Delta\phi = 120^\circ$ guiding mode appropriate for spatial focusing. Here, the microwave field is switched on when the synchronous molecule arrives at the first position of a

potential well where the field strength is 50% of the maximum value. It is switched off again when this molecule reaches the next position with 50% field strength within the same potential well (see also Figure 4).

For this guiding sequence, two different effects on the motion of the molecules occur. First, the molecules are focused onto the resonator axis that is chosen to coincide with the molecular beam axis. This keeps the packet together in the transverse direction. Second, as mentioned above, molecules that are ahead of the synchronous molecule will be decelerated by the applied microwave field while the molecules lagging behind will be accelerated. In total, the packet will be kept together both in longitudinal and transverse direction and perform a clockwise rotation in the longitudinal phase space (see inset of Figure 5). We designed our experiment such that a packet of 25 m/s slow molecules experiences almost exactly half a rotation until arrival in the detection zone, resulting in a very narrow peak with a temporal width of only 50 μs (Figure 5, lower trace and inset). This means, we have obtained nearly perfect spatial focusing down to a packet size of about 1.2 mm. The tight spatial focus goes along with a broader velocity distribution in the phase space (Figure 5, phase-space inset).

For certain applications such as controlled collision experiments or continuous loading of a trap, a tight velocity focus might be advantageous. This can, in principle, be achieved by reducing the electric field strength in order to reduce the phase-space rotation. This is prevented by severe transverse losses. As an alternative, additional switching can be introduced. If the microwave field is additionally applied when the synchronous molecule is close to the field nodes on the axis (first time switched on at $\phi_{1,1} = 0^\circ$ with the duration $\Delta\phi_1 = 20^\circ$, second time switched on at $\phi_{1,2} = 30^\circ$ with the duration $\Delta\phi_2 = 120^\circ$, and third time switched on at $\phi_{1,3} = 160^\circ$ with the duration $\Delta\phi_3 = 20^\circ$), the overall phase-space rotation can be reduced. The parts of the field potential close to the field nodes are longitudinally defocusing and can be used to adjust the overall rotation in the longitudinal phase space at the cost of some reduction in the phase-space acceptance. The resulting velocity focusing comes with a broader spatial distribution and is displayed in Figure 5, middle trace. The temporal width of the peak is significantly increased ($\sim$260 μs). From the phase-space inset we can see that the central part of the molecular packet has only a very small velocity spread of the order of 0.5 m/s centred around the mean longitudinal velocity of 25 m/s. This feature is the desired velocity focusing that affects only a small portion of the molecular packet. This is located around the dip that is visible in the high-resolution measurements. Using appropriately switched microwave fields, we can therefore deliberately choose the form of the generated packet of molecules in high-field-seeking states in the longitudinal phase space, i.e., for example by choosing velocity or spatial focusing or anything in between [26].

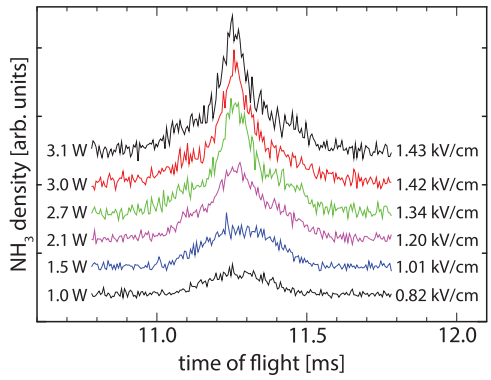

Figure 6. Microwave guiding of a 12 m/s slow ammonia packet using different microwave input powers. The traces have been given an offset for clarity.

Guiding can be extended to lower molecular velocities as well. In Figure 6, we show microwave guiding of a 12 m/s slow packet for different microwave input powers P_{MW}, but the same guiding sequence ($\phi_1 = 30^\circ$ and $\Delta\phi = 120^\circ$). In the top trace with the maximum input power, a nice spatially bunched packet of ammonia molecules is generated. With decreasing input power P_{MW}, the electric field E_{MW} in the cavity decreases according to $E_{MW} \propto \sqrt{P_{MW}}$ (see also Equation (2)). As a consequence, the molecular packet is transversally less confined, thus less molecules arrive in the detection region. (The integrated traces normalised with respect to the most intense peak obtained with 3 W of microwave power are 1 : 0.99 : 0.98 : 0.77 : 0.46 : 0.23). In addition, the achievable rotation in the phase space will decrease, resulting in not only less intense, but also wider packets of molecules.

A comparison of the guiding performance for different longitudinal velocities (12, 15 and 28 m/s) for $P_{MW} =$ 3 W is given in Figure 7. The ratio of the numbers of detected molecules using 12, 15, and 28 m/s slow packets, normalised to the most intense peak of the 12 m/s slow molecules, is 1 : 0.93 : 0.42, respectively. The number of detected molecules is lowest for the 28 m/s slow packet

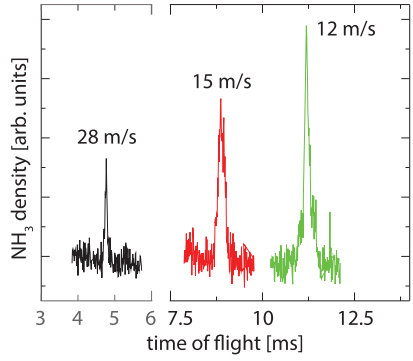

Figure 7. Time-of-flight profiles of microwave-guided ammonia packets travelling at 28 m/s, 15 m/s, and 12 m/s, respectively.

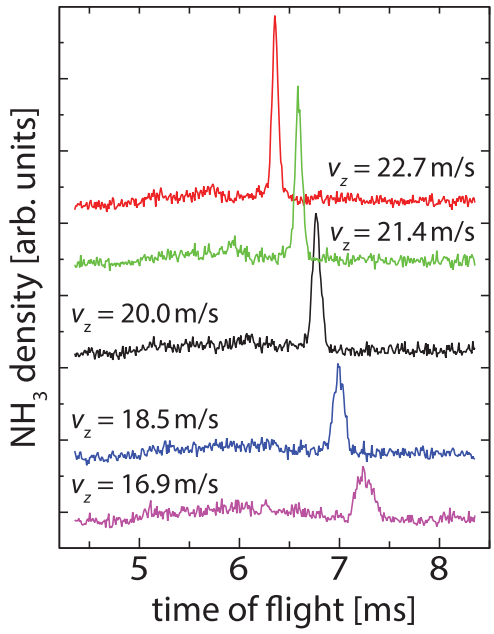

Figure 8. Microwave guiding, acceleration, and deceleration of molecular packets travelling at a mean initial velocity of 20 m/s inside the microwave decelerator (the data shown in this figure have already been discussed in Ref. [23]).

(FWHM $\approx 65\ \mu$s). The higher initial velocity reduces the time the molecules spend within the microwave fields, thus reducing the transverse focusing effect. The depth of the microwave trap is $h \cdot 236$ MHz in z- and x-directions ($\phi = 0$), but only $h \cdot 96$ MHz in the y-direction ($\phi = \pi/2$). The number of molecules per packet travelling at 12 and 15 m/s is comparable. However, under the respective experimental condition we are closer to spatial focusing for the 12 m/s slow packet, resulting in the rather narrow (FWHM $\approx$ 125 μs) and intense peak in the time-of-flight distribution. For 15 m/s the obtained peak width is somewhat broader (190 μs).

To extend our technique to deceleration and acceleration, we employ switching schemes that are similar to the guiding sequence but shifted longitudinally (see Figure 4). As a result, the longitudinal velocity of the synchronous molecule will be changed (i.e., the molecules are decelerated or accelerated). The switching sequences have to account for this change in the longitudinal velocity of the molecules in different stages. In Figure 8, the deceleration and acceleration measurements are shown starting from a 20 m/s slow packet of ammonia molecules using $P_{MW} =$ 3 W. The microwave switching sequences have the same microwave duration $\Delta\phi = 120^\circ$. However, the position when the field is switched on (ϕ_1) is varied. The middle trace shows the normal guiding mode with $\phi_1 = 30^\circ$ for comparison. The bottom traces demonstrate deceleration with $\phi_1 = 45^\circ$ and $\phi_1 = 60^\circ$, and final velocities of 18.5 m/s and 16.9 m/s, respectively. The two upper traces display

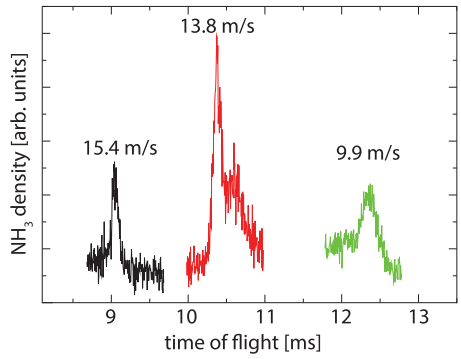

Figure 9. Microwave acceleration and deceleration of molecular packets travelling with a mean initial velocity of 12 m/s.

acceleration measurements with $\phi_1 = 0^\circ$ and $\phi_1 = 15^\circ$ and final velocities of 22.7 m/s and 21.4 m/s, respectively. The gain or loss in kinetic energy amounts to $h \cdot 100$ MHz ($\phi_1 = 15^\circ$ and $\phi_1 = 45^\circ$) and $h \cdot 201$ MHz ($\phi_1 = 0^\circ$ and $\phi_1 = 60^\circ$) per stage.

Figure 9 shows microwave deceleration and acceleration measurements starting from a 12 m/s slow beam of ammonia molecules with which we achieved the maximum deceleration, generating $^{14}NH_3$ molecules as slow as 9.9 m/s. This means, more than 30% of the kinetic energy has been removed. All switching sequences (deceleration and acceleration) share $\Delta\phi = 120^\circ$. ϕ_1 is varied from 40° for deceleration to $\phi_1 = 10^\circ$ and $\phi_1 = 20^\circ$ for two different acceleration experiments. This results in acceleration from 12 m/s to 15.4 m/s and 13.8 m/s and corresponds to a gain in the kinetic energy of 63.5% and 32.5%, respectively.

6. Conclusions and outlook

Our measurements show that microwave deceleration is an interesting and viable technique to even handle very slow molecular packets of molecules in high-field-seeking states. For these low velocities, longitudinal and transverse motion can no longer be assumed to be independent, which complicates stable deceleration to very low velocities or even to standstill. Furthermore, due to the low velocities, the molecular packet tends to spread out transversally, resulting in large losses during the free-flight zones. We could demonstrate deceleration of ammonia molecules in high-field-seeking states down to 9.9 m/s. To microwave-decelerate molecules to standstill and to subsequently trap them, larger field strengths would be needed and higher molecule numbers would be helpful. According to Equation (2), the microwave field strength depends on the quality factor Q of the resonator, the microwave power P_{MW} and the resonator volume V. Higher power could be achieved with travelling wave tube amplifiers, for example. A higher quality factor could be achieved by cooling the resonator to even lower temperatures [27], however, this would require helium as the cooling agent, and the current heat load on the order of

4 W might be difficult to handle for helium cryostats. For us, it appears to be the most feasible way to decrease the resonator volume by reducing the length of the cavity by a factor of 3, for example. For such a 40 mm long resonator, the $TE_{1,1,4}$ mode would be resonant at around 23.7 GHz and thus well suited for our experiments. This would result in an increase in field strength by $\sqrt{3}$, which would significantly improve the transverse focusing forces of the microwave decelerator. Due to the reduced number of stages, however, its deceleration/acceleration capabilities would be reduced. This naturally leads to a multi-resonator design, i.e., using several smaller resonators in a row. This will not only improve the deceleration and acceleration performance of the present set-up, but more importantly it will deepen the potential by a factor of $\sqrt{3}$ and thus more molecules should survive the passage through the microwave cavity.

We are convinced that the described properties of microwave deceleration of molecules in high-field-seeking states make it an interesting candidate for combining it with slow beams of buffer-gas-cooled molecules, for example. Depending on the respective experimental conditions, they offer very high molecule numbers of internally cold molecules with remaining longitudinal velocities of the order of 50 m/s. Microwave deceleration can be nicely applied to further decelerate these polar molecules in high-field-seeking states in order to trap them or exploit them for modern precision spectroscopy experiments [28]. It is interesting to compare microwave deceleration with travelling wave deceleration of polar molecules which has been realised first on a chip [29], even though it is so far only applicable to molecules in low-field-seeking states. This method has been scaled up in ring-electrode decelerators. Stable deceleration of low-field-seeking ammonia molecules down to standstill and subsequent trapping in one of the moving wells have recently been demonstrated [30]. While this recent work undoubtedly demonstrates the promising potential to handle low-velocity packets of molecules in low-field-seeking states (even those that will become high-field seeking at already low electric field strengths such as for the heavy molecules YbF and SrF, as the authors point out), this technique will not be applicable to molecules dominated by high-field-seeking states, and thus will again be restricted to rather specific molecules. The more general approach of microwave deceleration as we presented here will unrestrictedly allow for the stable deceleration of molecules in high-field-seeking states and thus also the molecular ground state, making it a unique and promising technique within the research field of cold molecules.

Acknowledgements

We thank Jens–Uwe Grabow, Boris Sartakov, and Wolfgang Jäger for helpful scientific discussions on various topics. This work has been supported by the ERC–2009–AdG programme under grant agreement 247142–MolChip, and the support of the Fonds der Chemischen Industrie via a Dozentenstipendium (MS).

References

[1] S.Y.T. van de Meerakker, H.L. Bethlem, N. Vanhaecke, and G. Meijer, Chem. Rev. **112**, 4828 (2012).
[2] S.D. Hogan, M. Motsch, and F. Merkt, Phys. Chem. Chem. Phys. **13**, 18705 (2011).
[3] M. Schnell and G. Meijer, Angw. Chem. Int. Ed. **48**, 6010 (2009).
[4] M.T. Bell and T.P. Softley, Mol. Phys. **107**, 99, (2009).
[5] J. van Veldhoven, J. Küpper, H.L. Bethlem, B. Sartakov, A.J.A. van Roij, and G. Meijer, Eur. Phys. J. D **31**, 337 (2004).
[6] E.R. Hudson, H.J. Lewandowski, B.C. Sawyer, and J. Ye, Phys. Rev. Lett. **96**, 143004 (2006).
[7] L. Scharfenberg, J. Klos, P.J. Dagdigian, M.H. Alexander, G. Meijer, and S.Y.T. van de Meerakker, Phys. Chem. Chem. Phys. **12**, 10660 (2010).
[8] M. Kirste, X. Wang, H.C. Schewe, G. Meijer, K. Liu, A. van der Avoird, L.M.C. Janssen, K.B. Gubbels, G.C. Groenenboom, and S.Y.T. van de Meerakker, Science **338**, 1060 (2012).
[9] H.L. Bethlem, G. Berden, and G. Meijer, Phys. Rev. Lett. **83**, 1558 (1999).
[10] T. Junglen, T. Rieger, S.A. Rangwala, P.W.H. Pinkse, and G. Rempe, Phys. Rev. Lett. **92**, 223001 (2004).
[11] F. Filsinger, U. Erlekam, G. von Helden, J. Küpper, and G. Meijer, Phys. Rev. Lett. **100**, 133003 (2008).
[12] M.R. Tarbutt and E.A. Hinds, New. J. Phys. **10**, 073011 (2008).
[13] S. Putzke, F. Filsinger, H. Haak, J. Küpper, and G. Meijer, Phys. Chem. Chem. Phys. **13**, 18962 (2011).
[14] H.L. Bethlem, A.J.A. van Roij, R.T. Jongma, and G. Meijer, Phys. Rev. Lett. **88**, 133003 (2002).
[15] K. Wohlfart, F. Grätz, F. Filsinger, H. Haak, G. Meijer, and J. Küpper, Phys. Rev. A **77**, 031404(R) (2008).
[16] J. van Veldhoven, H.L. Bethlem, and G. Meijer, Phys. Rev. Lett. **94**, 083001 (2005).
[17] M. Schnell, P. Lützow, J. van Feldhoven, H.L. Bethlem, J. Küpper, B. Friedrich, M. Schleier–Smith, H. Haak, and G. Meijer, J. Phys. Chem. **111**, 7411–7419 (2007).
[18] L. Holmegaard, J.H. Nielsen, I. Nevo, H. Stapelfeldt, F. Filsinger, J. Küpper, and G. Meijer, Phys. Rev. Lett. **102**, 023001 (2009).
[19] R. Fulton, A.I. Bishop, M.N. Shneider, and P.F. Barker, Nat. Phys. **2**, 465–468 (2006).
[20] S. Earnshaw, Trans. Cambridge Philos. Soc. **7**, 97 (1842).
[21] R. Hill and T. Gallagher, Phys. Rev. A **12**, 451 (1975).
[22] H. Odashima, S. Merz, K. Enomoto, M. Schnell, and G. Meijer, Phys. Rev. Lett. **104**, 253001 (2010).
[23] S. Merz, N. Vanhaecke, W. Jäger, M. Schnell, and G. Meijer, Phys. Rev. A **85**, 063411 (2012).
[24] H.L. Bethlem, F.M.H. Crompvoets, R.T. Jongma, S.Y.T. van de Meerakker, and G. Meijer, Phys. Rev. A **65**, 053416 (2002).
[25] BNL 10200–R, Vol. II, Brookhaven National Laboratory Selected Cryogenic Data Notebook (revised August 1980).
[26] F.M.H. Crompvoets, R.T. Jongma, H.L. Bethlem, A.J.A. van Roij, and G. Meijer, Phys. Rev. Lett. **89**, 093004 (2002).
[27] K. Enomoto, P. Djuricanin, I. Gerhardt, O. Nourbakhsh, Y. Moriwari, W. Hardy, and T. Momose, Appl. Phys. B **109**, 149 (2012).
[28] M. Schnell and J. Küpper, Faraday Discuss. **150**, 33 (2011).
[29] S.A. Meek, H. Conrad, and G. Meijer, Science **324**, 1699 (2009).
[30] M. Quintero-Perez, P. Jansen, T.E. Wall, J.E. van den Berg, S. Hoekstra, and H.L. Bethlem, Phys. Rev. Lett. **110**, 133003 (2013).